KEK Preprint 94-163
December 1994
H

Emulsion-Counter Hybrid Detector for the Study of Double Hypernuclei and the H-dibaryon

S.Aoki[5], S.Y.Bahk[2], K.S.Chung[3], S.H.Chung[3], O.Fukuda[4], C.H.Hahn[16], T.Hara[5], S.Hirata[6], K.Hoshino[1], M.Ieiri[7], T.Iijima[6], K.Imai[6], T.Ishigami[8], M.Kazuno[8], K.Kikuchi[4], C.O.Kim[9], D.C.Kim[3], J.Y.Kim[10], T.C.Kim[3], H.Kitamura[1], M.Kobayashi[1], M.Kobayashi[8], K.Kodama[11], Y.Maeda[2], A.Masaike[6], Y.Matsuda[5], F.Minakawa[8], M.Miyanishi[1], C.Nagoshi[13], M.Nakamura[1], S.Nakanishi[1], T.Nakano[6], K.Nakazawa[14], K.Niu[1], K.Niwa[1], H.Okabe[15], S.Ono[8], I.G.Park[3], M.S.Park[3], Y.Sato[4], H.Shibuya[8], H.M.Shimizu[6], J.S.Song[3], H.Tajima[1], R.Takashima[17], F.Takeutchi[18], K.H.Tanaka[7], M.Teranaka[19], I.Tezuka[4], H.Togawa[6], Y.Ueda[5], N.Ushida[11], S.Watanabe[8], C.S.Yoon[3] and J.Yokota[15]

[1] Department of Physics, Nagoya Univ., Nagoya 464, Japan.
[2] Wonkwang Univ., Iri 570-749, Korea
[3] Gyeongsang National Univ., Jinju 660-300, Korea
[4] Faculty of Education, Utsunomiya Univ., Utsunomiya 321, Japan.
[5] Physics Department, Kobe Univ., Kobe 657, Japan.
[6] Department of Physics, Kyoto Univ., Kyoto 606, Japan.
[7] National Laboratory for High Energy Physics, Tsukuba 305, Japan.
[8] Department of Physics, Toho Univ.,Funabashi 274, Japan.
[9] Korea Univ., Seoul 136-701, Korea
[10] Chonnam National Univ., Kwangju 500-757, Korea
[11] Aichi Univ. of Education, Kariya 448, Japan.
[12] Faculty of Education, Yokohama National Univ., Yokohama 240, Japan.
[13] Institute for Nuclear Study, Univ. of Tokyo, Tanashi, Tokyo 188, Japan.
[14] Faculty of Education, Univ. of Gifu, Gifu 501-11, Japan.
[15] Science Education Institute of Osaka, Osaka 558, Japan.
[16] Changwon National Univ., Changwon, Korea
[17] Kyoto Univ. of Education, Kyoto 612, Japan.
[18] Kyoto Sangyo Univ., Kyoto 603, Japan.
[19] Department of Physics, Osaka City Univ., Osaka 558, Japan.

Submitted to Review of Scientific Instruments.

National Laboratory for High Energy Physics, 1994

KEK Reports are available from:

Technical Information & Library
National Laboratory for High Energy Physics
1-1 Oho, Tsukuba-shi
Ibaraki-ken, 305
JAPAN

Phone: 0298-64-1171
Telex: 3652-534 (Domestic)
(0)3652-534 (International)
Fax: 0298-64-4604
Cable: KEK OHO
E-mail: LIBRARY@JPNKEKVX (Bitnet Address)
library@kekvax.kek.jp (Internet Address)

Abstract

An emulsion-counter hybrid detector has been constructed for an experiment (E176 at KEK) aimed at searching for double hypernuclei and the H-dibaryon. The (K^-,K^+) reaction from nuclei in the emulsion target is identified by a K^+ spectrometer comprising a magnet, tracking chambers, an aerogel Cherenkov detector, a time-of-flight hodoscope and silicon microstrip detectors. The position of a K^+ track in the emulsion can be predicted with high accuracy by using silicon microstrip detectors. In this method, the (K^-,K^+) vertices and stopped Ξ^- events in the emulsion can be studied with much higher statistics and reliability than before. The spectrometer and the emulsion target system are described together with their performances.

1 Introduction

Since the H-dibaryon (I=J=0 ssuudd) was first predicted to be stable against strong decay [1], many theoretical studies have been performed, many of them suggesting the existence of a stable H-dibaryon [2]. The H-dibaryon has a key importance in studies of multiquark systems and the confinement aspect of QCD, since the H-dibaryon is expected to be bound due to the QCD colormagnetic interaction between quarks. Moreover the existence of the H-dibaryon is related to the possibility of strange quark matter and a quark star [3]. Although there have been a few experiments which searched for the H-dibaryon [4], none seems to have been conclusive. On the other hand, there were two old emulsion data used to claim the observation of the weak decay of double hypernuclei [5]. It is argued that the existence of such a weakly decaying double hypernucleus can exclude the H-dibaryon in the mass region of $1900 \sim 2200$ MeV [6]. The statistics and reliability of the old emulsion data are, however, too poor to exclude the existence of the H-dibaryon. It is, therefore, also very important to confirm the existence of double hypernuclei as well as the H-dibaryon. Even today the nuclear-emulsion detector is unique, having a sufficient position resolution to detect very short tracks of hyperfragments. An emulsion-counter hybrid detector has therefore been constructed to search for double hypernuclei as well as the H-dibaryon.

In the emulsion-counter hybrid technique, a specific reaction is selected by analyzing counter data; the vertex of the selected event is then studied in detail using the emulsion, taking advantage of its high position resolution (1μm). To locate a selected event among many background tracks in the emulsion, a high-resolution detector, such as a silicon microstrip detector, is usually employed. The emulsion-counter hybrid technique can greatly improve the statistics and reliability of the data, compared to the old-type emulsion measurement. Especially, this technique makes it possible to study rare events in the emulsion.

It has been successfully applied for the detection of short-lived particles, such as charm and beauty hadrons, with high-energy beams at CERN and Fermilab [7]. For the first time we have applied this technique to a low-energy experiment.

The emulsion-counter hybrid detector described in this paper comprises a K^+ spectrometer and an emulsion target. The (K^-,K^+) reactions from nuclei in the emulsion are measured with a K^+ spectrometer, which is a magnetic-spectrometer with an aerogel Cherenkov detector and a TOF hodoscope for particle identification. In this reaction, strangeness of -2 is transferred to the target nucleus, and a double hypernucleus or the H-dibaryon can be produced directly[8]. It is expected that the (K^-,K^+) reaction proceeds mainly through a two-body process, $K^-(p) \rightarrow K^+\Xi^-$, in nuclei. Since the Ξ^- from this reaction has a larger momentum (> 500 MeV/c) than the nuclear Fermi momentum, a large fraction of the Ξ^- are scattered out of the nuclei. Although most of the produced Ξ^- decay in flight, some Ξ^- are expected to stop in the emulsion. Then, a stopped Ξ^- is absorbed by a nucleus through a Ξ^- atomic state. Due to the Q-value (28 MeV) of the conversion process, $\Xi^-p \rightarrow \Lambda\Lambda$, a light hyperfragment can be emitted and observed as a short track with a decay vertex. If a light double hypernucleus is emitted, it should be identified by its sequential weak decay. If the H-dibaryon exists and its mass is less than that of two Λ, a nucleus with S=-2 (Ξ^- hypernucleus or double Λ hypernucleus) can decay by emitting an H-dibaryon through a strong interaction, $\Xi^-p \rightarrow H$ or $\Lambda\Lambda \rightarrow H$, decaying into Σ^-p near to the stopping point of the Ξ^- (within 1 mm). The H-dibaryon can be identified in the emulsion as a neutral track. This is possible if the lifetime of the H-dibaryon is about the same or less than that of a hyperon ($< 10^{-10}$ sec).

Because of the small cross section of the (K^-,K^+) reaction, only a few candidates of the (K^-,K^+) reaction and Ξ^--capture events were found in the old-type emulsions exposed to K^- beams, where both K^- and K^+ were not identified in most cases.[5,9] On the other hand,

the emulsion-counter hybrid detector enables us to study hundreds of times more (K^-,K^+) reaction and Ξ^--capture events in the emulsion, where both K^- and K^+ are clearly identified by the counters. In addition to searching for double hypernuclei and H-dibaryon, it will also reveal the general features of the (K^-,K^+) reaction and Ξ^--capture at rest for the first time. In the following sections, the K^- beam line, the K^+ spectrometer, the silicon microstrip detector, the emulsion target system and their performances are described.

2 K^- beam line

A separated 1.66 GeV/c K^- beam is provided by the K2 beam line of the 12GeV Proton Synchrotron at the National Laboratory for High Energy Physics (KEK). This beam line was slightly modified from the original design [10] so as to improve the K/π ratio and to accommodate detectors. The total length of the beam line is 25.7m, which is shorter than the original one by 2.2m. The beam line is shown in Fig.1, together with the detectors. It comprises a production target, dipole, quadrupole and sextupole magnets and an electrostatic mass separator (6m long). The K/π ratio is crutial for the emulsion experiment because the emulsion is sensitive to all charged particles. The statistics of the (K^-,K^+) reaction for a given amount of emulsion is limited by the total number of beam particles, not only by the K^- particles. The production target is a platinum bar (2mm in height, 6mm in width and 60mm in length). The magnification of the target image at the position of the mass slit is 0.88 in the vertical direction. The electrostatic field of the separator has typically been 65 kV/cm during an experiment, and separated K^- and π^- by 5.6 mm at the mass slit. We have found that the emittance of the K^--beam at the target position is smaller than the background π^-. One of the reasons is that some background π^- come from Ks-decay. A collimator made of 100cm thick iron placed just after the final focusing magnet(Q7) has

improved the K^-/π^- ratio while cutting the beam halo. The typical value of the K^-/π^- ratio is 1/3 at an intensity of 3x10^3 K^-/spill. The size of the beam at the target is 15 mm (FWHM) in the vertical direction and 17.5 mm (FWHM) in the horizontal direction, which is sufficiently small to be covered by silicon microstrip detectors ($50\times50mm^2$). As shown in Fig.1, four identical MWPCs (BPC1-4) are used for tracking the beam particles as well as for tuning the beam line [11]. An aerogel Cherenkov counter (AC1) and TOF counters (T1,T2) are used to identify the beam particle (described in the next section).

3 K^+ spectrometer

3.1 Design principle of the K^+spectrometer

Scattered K^+ are detected with a K^+ spectrometer comprising a magnet (0.7 Tesla.m), silicon microstrip detectors, wire chambers (PC1-3, DC1-3), an aerogel Cherenkov counter (AC2) and trigger and TOF hodoscopes. An overview of the spectrometer is shown in Fig.2. The design principle of the spectrometer is as follows: (1) Since the emulsion is sensitive to all of the beam particles and the amount of emulsion is limited practically, the acceptance of the spectrometer should be as large as possible in order to detect the (K^-,K^+) reaction as much as possible. We detect the (K^-,K^+) reaction from various nuclei in the emulsion, and the K^+ momentum is expected to be smeared by the nucleon Fermi motion in nuclei. A large momentum acceptance is, therefore, rather more important than the momentum resolution. (2) The position and angle of scattered K^+ should be measured with high precision in order to locate K^+ tracks in the emulsion. (3) Since the (K^-,K^+) reaction has a rather small cross section compared with the (K^-,π^+) reaction and others, particle identification is crucial in this experiment. The yield ratio of K^+ to π^+ and protons is less than 1/100. In order to identify K^+ unambiguously, π^+ and protons should be rejected at the level of 10^{-4} with

aerogel Cherenkov detectors and TOF counters. (4) The inflight decay of the scattered K^- in the spectrometer could be background. A redundancy of the tracking chamber is quite necessary in order to reject these events without loosing tracking efficiency. (5) To minimize K^+ decay inflight, the path length of the spectrometer should be as short as possible. The spectrometer was thus designed to have a large acceptance (0.15 str) and a moderate momentum resolution ($\Delta p/p$ = 2.5%(rms) at p=1.0 GeV/c).

3.2 Magnet and tracking chambers

The spectrometer magnet is a window-frame-type dipole magnet having an aperture of 40 cm in height and 80 cm in width. It has 8 cm thick end-guard plates of larger aperture. The shape of the pole is rectangular and its length is 70 cm. The distance between the target and the center of the magnet is 99.1 cm, and the solid angle of the magnet aperture is 0.18 str. The central field is 10 kG during an experiment, which is far below saturation. The bending angle is about 250 mrad for 1.1 GeV/c, which is a typical K^+ momentum for Ξ^- production from a proton target. The incident K^- beam of 1.66 GeV/c is deflected by -160 mrad. A map of the magnetic field was obtained at several excitations for the past experiment [12]. We have used the existing data of those field measurements for momentum reconstruction in the data analysis.

The locations of the MWPCs and drift chambers are shown in Figs.1 and 2, and their parameters are summarized in table 1. The scattered particles are detected with three sets of MWPCs(PC1-3) and three sets of drift chambers(DC1-3). In the present configuration, the beam goes through most of the chambers and the rate ocaisionally becomes high. Since the MWPC can withstands high rate, and the drift chamber has a better position resolution, both types of chambers were used. The PC2 has three planes (x,y,u) to resolve the stereo ambiguity of multiple tracks. Both PC1 and PC2 have carbon-coated cathode planes that

are the same as the BPCs. For the PC3, the cathodes are aluminized mylar glued to 10mm thick honeycomb boards. The anode wires in the y-plane are supported by a vinyl-covered copper wire in the middle so as to avoid any instability due to the electrostatic force. These MWPCs are operated with the magic-gas-mixture of argon (73%), isobutane (24%), freon (0.5%) and methylal (3%). The DC1 is located at the same place as PC1. This duplication is important in order to measure the angle of a scattered particle precisely and reliably. The DC1 has just one plane for both x and y, and the left-right ambiguity is resolved by using PC1 and PC2. The position resolution of DC1 was measured by using a set of silicon microstrip detectors (described in sect.4). The resolution of DC1 was 210 μm (rms) and that of PC1 was 450 μm (rms). The DC2 and DC3 are identical chambers, except that the cathodes are aluminized mylar for DC3 and TiO-coated mylar for DC2, both glued onto a 2 cm thick acryl-foam board. They have double sense wires separated by 1 mm in order to resolve any left-right ambiguity. The typical position resolution is 300 μm (rms). The drift chambers are operated with a mixed gas of argon(50%) and ethane(50%). In addition to the chambers, we have used silicon microstrip detectors and the TOF hodoscope as tracking devices. A position resolution of 12mm(rms) has been obtained from the timing difference between two photo-tubes on both ends of a scintillator.

3.3 Particle identification detectors

Particle identification is made by using the aerogel Cherenkov counter and the TOF measurement. The AC1 is placed 75cm upstream of the target to identify K^- beam. Two layers of silica aerogel blocks (15 x 15 cm and 3 cm thick) are installed in a box. The Cherenkov light is reflected by a 45° mirror and detected by a 5 inch quantucon tube (RCA8854). The index of the aerogel for the AC1 is 1.04, which has been confirmed by measuring the threshold momentum of a pion beam. The average number of detected photo-electrons was 6.0 for

1.66 GeV/c pions, which is almost consistent with the measured value of its pion detection (rejection) efficiency (99.3%). The AC2 is located between PC1 and PC2 to separate scattered K^+ and π^+. The silica aerogel radiator for AC2 has a sensitive area of 15cm (height) × 25cm (width) and its total thickness is 9.5cm. To avoid magnetic fields, a 50 cm long air light-guide surrounded by aluminized mylar is employed for light collection to the two photo-tubes (RCA8854). The index of the aerogel for the AC2 is 1.06. The average number of detected photo-electrons is 4.4 for a 1.0 GeV/c pion, and its detection efficiency is 98.7%. Nitrogen gas is provided to both AC1 and AC2 to avoid deterioration of the aerogel.

Two timing counters (T1,T2) are located at 587.7cm and 56.1cm upstream of the target position, respectively. They are 5 mm thick plastic scintillators (NE pilot-U) directly viewed by fast timing phototubes (Hamamtsu R2083) on both ends. The area of the scintillator is 10cm (width) x 5 cm (height) for T1 and 5cm x 5cm for T2. The time difference between T1 and T2 is measured in order to identify the beam particles. The TOF(T2-T1) resolution is 85psec (rms), whereas the TOF difference of K^- and π^- is 700psec. Thus, any misidentification of π^- as K^- is on the order of 10^{-6} due to both the AC1 and TOF measurements. The time difference between the T2 and the TOF hodoscope is measured in order to identify scattered particles. The TOF hodoscope is located 2.7 m downstream from the target, and comprises 14 plastic scintillators (Kuraray SCSN38). By using a beam particle, the performance of the TOF counters was studied for various sizes of the scintillator and several phototubes to optimize the design [13]. The size of each scintillator is 110cm (height) × 12cm (width) × 3cm (thickness) and it has fish-tail light guides and 2-inch phototubes (Hamamatsu H1949) on both ends. The signal from each phototube is split into a discriminator and ADC. The leading-edge discriminator and CAMAC TDC are used for the time measurement together with the ADC information.

In an off-line analysis, a correction due to both the position and pulse height is made

to obtain the timing at each counter, $< t >$, by using the following formula:

$$t_u^c = t_u + k_u/\sqrt{a_u}, \quad t_d^c = t_d + k_d/\sqrt{a_d} \tag{1}$$

$$< t >= (t_u^c + t_d^c)/2 + C\,|t_u^c - t_d^c| \tag{2}$$

,where $t_u(t_d)$ and $a_u(a_d)$ are the timing(TDC) and pulse height(ADC) of the signal from the phototube on each end of a scintillator (here, we denote u and d). The coefficients k and C are determined so as to minimize the TOF resolution. (We take C=0 for T1 and T2 because of their small sizes.) The timing and resolution of each TOF counter is routinely calibrated using a pion beam. A typical value of the TOF resolution obtained with a pion beam is 90 psec(rms), which is quite satisfactory.

3.4 Trigger system

A trigger hodoscope (TH) is placed at the front edge of the magnet pole. It comprises 8 scintillation counters segmented in the horizontal plane. The size of each scintillator is 4.2cm(width)x 22cm(height)x 2mm(thickness). They have long light guides on one end and are viewed by 1-1/8 inch phototubes (Hamamatsu R1398). The hodoscope was used to form the 8×14 matrix coincidence with the TOF hodoscope so as to identify the charge of scattered particles for the trigger logic. The matrix is determined to select a positively charged particle by using the result of a Monte-Carlo simulation. A scintillation counter (BV) is placed at the same position as the trigger hodoscope to kill any noninteracting beam particles. This is useful for reducing the trigger rate by vetoing fake events due to the decay of the K^- beam particles in the magnet. The size of the scintillator is 4 cm square and 2mm thick, and is viewed with a 2 inch phototube (Hamamatsu R2490). The AC1 is always in the trigger to select K^- in the beam. The AC2 is usually not in the trigger to also detect the (K^-,π^+) reaction. Thus, the trigger requirement is that an incident particle is K^- and

charge of at least one scattered particle is positive. The typical trigger rate was about 40 events/spill, mostly due to the (K^-,p) and (K^-,π^+) reactions and the decay of scattered K^- in the spectrometer.

3.5 Performance of the spectrometer

The performance of the spectrometer was studied by using various beam particles at various energies as well as scattered particles from especially a proton target. The track reconstruction was made using a spline-fit method [14]. The scattering angle, vertex position, path length and momentum of each particle were obtained. With the use of TOF and aerogel Cherenkov information, the mass of the particle was calculated. Details concerning the analysis are described elsewhere [15]. A mass spectrum of scattered particles from the emulsion target is shown in Fig.3a (whole momentum region) and b ($P = 0.9 \rightarrow 1.2 GeV/c^2$). The K^+ is clearly separated from the pion and proton. The mass resolution is about $30 MeV/c^2$ (rms) for K^+ in the high-momentum region. The misidentification of π^+ as K^+ is less than 0.1% due to two different particle-identification detectors. The misidentification of protons as K^+ was estimated to be typically less than 1%, depending on the cut parameters in the off-line analysis [16]. The proton rejection factor is about 1×10^{-5}. The momentum spectrum for the K^+ from the emulsion target is shown in Fig.4. The peak at $P = 1.1 GeV/c$ was well reproduced by the Monte-Carlo calculation (dotted line), assuming the quasi-free reaction, $K^- + (p) \rightarrow K^+ + \Xi^-$, from emulsion nuclei [17]. The (K^-,K^+) reaction from a carbon and CH_2 target has also been measured. A comparison of the K^+ momentum spectra for these two targets provides the spectrum for the proton target. Fig.5 shows the missing-mass spectrum of the $K^- + p \rightarrow K^+ + X$ reaction. The peaks corresponding to Ξ^- and $\Xi^{-*}(1530)$ can be clearly seen. The observed values of the masses of Ξ^- and $\Xi^{-*}(1530)$ are the same as the reported values. The mass resolution of the Ξ^- peak is 22 MeV/c^2(rms). This is

consistent with the momentum resolution of the K^- beam (Δp/p=1.4%) and that of K^+ spectrometer (2.5% at P=1.1GeV/c). The latter is largely limited by multiple scattering mainly in the AC2.

The acceptance of the spectrometer was obtained by the Monte-Carlo simulation. Fig.6 shows the acceptance vs momentum of a scattered particle. The acceptance is 0.15 str. above 1.1 GeV/c and gradually decreases below it. It should be noted that the spectrometer has a large momentum acceptance. The cross section of the $K^- + p \rightarrow K^+ + \Xi^-$ reaction was obtained as

$$\langle d\sigma/d\Omega_L \rangle^f = 35 \pm 4\mu\, b/sr.$$

Note that the cross section dedicated by $\langle d\sigma/d\Omega_L \rangle^f$ means the cross section averaged over the laboratory forward angular region between 1.7° and 13.6°. This value is consistent with the existing data within the errors [18].

4 Silicon microstrip detector

In order to find the (K^-,K^+) vertex and follow the Ξ^- track to its stopping position in the emulsion, the K^+ track should first be identified in the emulsion sheet of the downstream end of the stack and followed up to the (K^-,K^+) vertex through the sequence of the emulsion sheet. Since the emulsion is a storage-type detector, many off-timing tracks are recorded. In order to find the predicted K^+ track in the high track density, the accuracy of the predicted position of the K^+ is crucial. Therefore the emulsion stack is sandwiched between silicon microstrip detectors (SSD1-4) which measure the position of both incoming K^- and outgoing particles with high precision. This is the key detector used to connect the counter information and the tracks in the emulsion. The locations of the SSDs and the emulsion target are shown in Fig.7. The sensitive area of the SSD is 50x50 mm^2, and the

thickness is 300 μm. The strip pitch is 42 μm. It is fabricated on a 54cm × 33cm pc board.

We have employed the method of capacitive charge division for the readout in order to reduce the number of readout electronics without affecting the position resolution [19]. Every third strip is connected to the pc board and readout electronics, while all other strips remain floating. The hit position is obtained by calculating the ratio of the collected charge of the adjacent readout strips. To supply a bias voltage to the floating strips, a MOS gate structure has been developed and is being utilized [20]. A signal from the readout strip is fed to a preamplifier on the pc board. Each pc board has 48 8-channel preamplifier chips (Lecroy HQVS10). It is a FET charge amplifier with a rather long time constant (4 μsec) and a high conversion gain (0.5 V/pC). The output signals from the preamplifiers are sent through 5 m long shielded flat cables to shaping amplifiers which are designed for this experiment. The voltage gain is 20 and the shaping time is 250 nsec. The output pulse is finally fed to a TKO-ADC [21]. The total number of ADC channels is 1200. In order to prevent noise from outside, the SSDs and their readout electronics, including ADCs, are located inside of an aluminum hat. It is used as an electromagnetic shield and to also keep the temperature constant for the emulsion target. The typical noise level during the experiment is 800 electrons(rms), where the capacitance of the strip is around 10 pF. This noise level is low enough compared with the signal, since the average number of electron-hole pairs produced by a minimum ionizing particle is 22000.

The intrinsic position resolution of this detector was measured to be 16 μm (rms) by using two SSDs,the strip pitch of which is much finer (12.5 μm), as shown in Fig.8. The performance of the vertex detector system including DC1 and PC1 can be checked with the emulsion. The accuracy of the position of a K^+ track at the downstream end of the emulsion target predicted by the vertex detector system was estimated to be less than 30μm, according to emulsion scanning (described in sect.7.1). The position resolution of the vertex

detector system is sufficient to locate a track in the emulsion with high efficiency.

5 Emulsion target

5.1 Structure of the emulsion target

An emulsion stack is used as a target, a degrader for produced Ξ^- and a detector for hyper-fragments and particles from vertices of both the (K^-, K^+) reaction and stopped Ξ^-. We have employed the vertical type, where a beam is irradiated perpendicularly to the surface of the emulsion sheets. This type is especially suitable for connecting any tracks detected by a counter system to the emulsion under a high track density, and to accumulate a large number of interactions.

The thickness of the target was determined in consideration of the ratios of stopped Ξ^- to the produced Ξ^- and the incident K^-. By a Monte-Carlo simulation we have estimated the ratio for emulsions of various thickness, assuming that the Ξ^- is produced by a quasi-free (K^-,K^+) reaction from the emulsion nuclei. The ratio tends to be saturated above 5 cm. The secondary interactions in the emulsion increase linearly as the thickness increases. We have also estimated the ratio of stopped Ξ^- to the incident K^- corrected by secondary interactions (Fig.9). The thickness of the emulsion target was determined to be 5 cm, which is about a 0.13 interaction length. The expected ratio of the stopped Ξ^- events to the total Ξ^- events is about 10%, according to the Monte-Carlo simulation.

Each emulsion stack comprises 42 thick emulsion sheets and one thin emulsion sheet (Fig.10). The size of the sheet is 23 × 23 cm^2. A thick sheet has 550 μm thick emulsion layers on both sides of a 70 μm thick polystyrene base. A thin sheet has 70 μm emulsion layers on both sides of a 500 μm thick lucite base in order to avoid any degradation of the angular resolution due to the distortion in the emulsion layer. Therefore, it is placed at

the bottom (downstream end) of the stack for the connection of K^+ tracks from outside of the stack. Emulsion sheets, i.e. 42 thick sheets and one thin sheet, were packed into one emulsion stack by the "ORIGAMI" method, which is vacuum packing with 200 μm thick multi-laminated paper. There is no material between each sheet in order to avoid multiple Coulomb scattering. The flatness of a stack is kept to be within ± 100 μm.

The emulsion was delivered in gel form and processed at the Nagoya University to make emulsion sheets just before the exposure. In total, 31 litters of nuclear emulsion gel (FUJI ET-7B) was used to make the emulsion sheets, ending up with 14 emulsion stacks. Due to loss during the process, the ratio of the effective gel to the prepared gel was 80%. Table 2 shows the composition of the emulsion (FUJI ET-7B). The density of our emulsion is 3.45 g/cm^3.

5.2 Exposure density and "changeable sheet"

The maximum density of hadron interactions in an emulsion is limited by the optical condition of the emulsion sheet for scanning. The evaporation tracks from beam interactions obscure the emulsion sheet. From past experience, the upper limit is about 10^4 interactions $/cm^3$. Since the interaction length is about 40 cm, the maximum beam density was estimated to be around $10^6/cm^2$. In this experiment, the exposed beam densities were $6 \times 10^5/cm^2$ for nine target stacks and $9 \times 10^5/cm^2$ for five stacks. In total, 3×10^8 interactions were recorded in emulsion targets. Since the K/π ratio is about 0.3, the number of K^- interactions in the fiducial volume is $\sim 6 \times 10^7$.

In order to locate K^+ tracks in the emulsion target reliably and quickly at such a high beam density, we have used an additional emulsion sheet, which is called a changeable sheet. The changeable sheet has 70 μm thick emulsion layers on both sides of a 500 μm

lucite base. It is vacuum-packed with laminated paper. The changeable sheet is attached to the downstream surface of the emulsion stack by a vacuum chuck. It is changed 10 or 12 times for an exposure of each emulsion stack without removing the target stack from a target mover. By this new technique, the density of the background track in the changeable sheet, where the K^+ track has to be located, was reduced to be 1/10 of a target stack in the case of a low exposure density ($6 \times 10^5/cm^2$) and 1/12 in the case of a higher exposure density ($9 \times 10^5/cm^2$).

5.3 Alignment of the target

In order to obtain an accurate alignment between each changeable sheet and the emulsion stack, fiducial marks are recorded by collimated X-rays (maximum energy of 67 keV) using a thin cross-window collimator. The X-ray beam penetrates a changeable sheet and the emulsion sheets at the downstream end of the target stack. Then, fiducial marks are printed on both a changeable sheet and the emulsion sheets of the target stack. The mark on the target stack is multiply exposed to X rays as many times as the number of changeable sheets. However, the X-ray mark is not diffused because of the good accuracy of the target mover compared to the width of an X-ray collimator. The X-ray generator is fixed to the end-guard of the magnet. Since the position of the X-ray generator and the collimator is fixed during the exposure of all emulsion stacks, the position of the X-ray marks provides a common coordinate for all changeable sheets and emulsion stacks.

The target mover, beam SSDs and the other detectors around the target are installed on a high-precision granite table in order to suppress any change in the relative positions caused by a fluctuation of the environment, and to provide a coordinate reference for the alignment between the target mover and the SSDs. The alignments of the target mover and the SSDs were performed using a laser at an accuracy of 100 μm, by using the flat surface of

the granite table as a reference. The space between the changeable sheet and the VSSD(X) was set to be 5 mm. The relative alignment between the SSDs and the chambers was checked with a straight beam without the emulsion target.

5.4 Exposure of the emulsion target

During exposure, a target stack is mounted on a computer-controlled high-precision holder, which is called a target mover. In order to obtain a uniform exposure density, a micro-computer monitors the beam intensity in each beam spill and drives the target in the vertical direction by a step proportional to the beam intensity after the end of each beam spill. After one vertical scan of the exposure, the target is driven in the horizontal direction by 10 mm step, and the vertical scan is repeated. These processes are repeated until the whole surface (23 cm $\times$ 23 cm) is exposed. Such an exposure has been repeated as many times as the number of changeable sheets. The fluctuation of the exposed beam density in the target stack was less than 10%. The position (x and y) of the emulsion target was measured using high-precision position-encoders, and was recorded on magnetic tape together with counter data at each spill. The accuracy of the position measurement was 1 μm in the short term and 10 μm in the long term.

6 Data acquisition system

A schematic diagram of the data-taking system is shown in Fig.11. The timing (TDC) and pulse height (ADC) information is encoded into the address and digitized value, and stored into a buffer-memory module in the main crate of the CAMAC system, event by event during a spill time. Signals from MWPCs are fed to amp-discriminator cards located near to the counters through flat cables. The output signals of the cards are sent to latch

modules through $\sim$ 20 m twist-pair cables. The hit patterns in the latch modules are encoded into the wire address and transferred into a buffer memory. Signals from the SSDs are read by the TKO-ADC system. A 32-ch ADC module was developed for the present experiment. Pedestal subtraction and threshold discrimination for each channel is possible. Each threshold value is set to be $\sim 2.5\ \sigma$ of the pedestal peak. The data is transferred into a buffer memory module (MP) in a camac crate linked by a interface module (CH). Signals from drift chambers are also read by the TKO system, which is operated in the common-stop mode. The position of the target-mover is read by a CAMAC 16-bit input register module at the beginning of each spill.

All of the data stored in the buffer-memory modules are transferred to a computer after each spill. The data-taking system is controlled by a minicomputer (DEC μVAX) through a crate controller (Kinetic 3922) in the CAMAC main crate. The typical event size is about $200 \sim 300$ of 16-bit words.

The online data-acquisition and monitoring program is based on KEKV, which was developed at KEK. The real-time I/O subprocess controls the data-acquisition system (start and stop), and transfers the data into a region of the random-access memory, called the "V-buffer", which is shared with other processes. All the data written on "V-buffer" are continuously recorded on magnetic tape. Some portion of the data are analyzed for on-line monitoring at a typical sampling ratio of about 15%. The performance of the detectors is monitored by histograming a large number of data, such as the ADC and TDC distributions, counter-hit distributions, etc. Furthermore, several physical quantities, such as the momenta of the outgoing particles, the vertex points of the interactions, and even the mass of outgoing particles, are also obtained in the on-line analysis. In addition to data-taking, the μVAX is used to set the parameters of the TKO-ADCs for the SSDs.

7 Emulsion Analysis

In order to locate a predicted (K^-,K^+) interaction, we have applied the "SCAN-BACK" method instead of the traditional volume scanning method. The predicted vertex position of the (K^-,K^+) reaction obtained from the data of the SSDs and the chambers has a quite large error caused by multiple Coulomb scattering in the emulsion target. Moreover, a typical (K^-,K^+) event in the quasi-free region has a few evaporation tracks. Therefore, it is almost impossible to find the predicted vertex of the (K^-,K^+) reaction by the volume-scanning method.

The "SCAN-BACK" is performed as follows. At first, on a changeable sheet, a predicted K^+ track is searched and located by the semi-automatic scanning system [22]. Secondly, the located K^+ candidate track is connected from the changeable sheet to the target stack and traced back upstream to the primary interaction point. Since the track density and the interaction density is high and the (K^-, K^+) interaction usually has no extra track to compare with counter data, one mistake in the location procedure may lead to an incorrect interaction point. We have therefore checked the reliability of the SCAN-BACK method in several ways.

7.1 Analysis on the changeable sheet

The error (Δ_x,Δ_y) of the predicted position of K^+ on a changeable sheet is given as

$$\Delta_{x,y} = [(\delta\theta_{x,y} \times L_{x,y})^2 + (\delta L_{x,y} \times \theta_{x,y})^2 + \delta(SSD)^2 + \delta(MVR)^2 + \delta(Xray)^2]^{1/2}, \quad (3)$$

where $\delta\theta_{x,y}$ is the error in the angle of a track measured by the vertex detectors, which is about 1.5 mrad. for 1 GeV/c K^+. $L_{x,y}$ is the distance between a changeable sheet and SSDs ($L_x = 5mm$ and $L_y = 15mm$); its error ($\delta L_{x,y}$) is about 100 μm. The $\delta(SSD)$, $\delta(MVR)$

and $\delta(Xray)$ represent the position resolution of the SSDs (16 μm), the accuracy of the target mover (10 μm) and the reading error of the X-ray mark (30 μm), respectively. Then, Δ_x and Δ_y were estimated to be less than 50 μm. Since the $\delta(Xray)$ is a common error for the events on the same changeable sheet, it becomes negligible after locating several tracks. Without $\delta(Xray)$, they were estimated to be 24 μm and 31 μm, respectively.

We have scanned an area of 300 $\times$ 350 μm^2 on the changeable sheet for each K^+ track. This is sufficiently large compared with the error in the predicted position. If the discrepancy of the angle of the emulsion track is smaller than the sum of the errors of the emulsion measurement (5 mrad) and counter measurement (1 mrad), we consider that the predicted track has been found. More than three reference tracks belonging to other obtained events (mostly π^+ or p) predicted around the K^+ track are scanned at the same time for a further confirmation of the locationing.

As a result of sample scanning, a good candidate track was found in 93% of the predicted events. About 2% of the events had double candidate tracks and 5% had no candidate. Therefore, the efficiency of finding the K^+ track on the changeable sheet is 95%. Figs.12a and b show the distribution of the difference between the position of a track predicted on the changeable sheet by the counter system and that actually found in the emulsion. The results show that the position resolutions are 22 μm in the horizontal direction and 31 μm in the vertical direction, respectively. These values are consistent with the estimation described above.

K^+ tracks are connected from a changeable sheet to the thin emulsion sheet (downstream end) of the target stack by using the X-ray marks as the coordinate references. This connection is performed using a semi-automatic scanning system with a large-stroke (25 $\times$ 25 cm^2) stage. This connection has also been confirmed by simultaneously connecting the

reference tracks described above.

7.2 Analysis in the target stack

From a thin sheet to a thick sheet and from a thick sheet to a thick sheet, a K^+ track is traced back until finding the interaction point. The rate of a misconnection in this procedure was estimated as follows. Twenty arbitrary tracks having a similar slope to a typical K^+ track were picked up on a changeable sheet and traced back in the target stack. As a result, 7 tracks passed throughout the target stack, 10 tracks reached to the vertices of e^+e^--pair creation and 3 tracks arrived at the interaction vertices of beam particles. By assuming that the found e-pairs and through-out tracks in any location were caused by a misconnection, the rate of the misconnection could be estimated. As for the interaction vertex, we could estimate the number of fake interactions due to misconnections, which are different from the predicted ones as,

$$(N_{ep} + N_{th}) \times (3/(20-3)), \tag{4}$$

where N_{ep} and N_{th} are the number of e-pair events and through-out tracks found in the scanned events, respectively.

In a sample scanning of the predicted events, we located 229 interaction vertices in our emulsion. In addition to these, 19 e-pair and 15 through-out events were found. The number of fake interaction events among the located 229 interaction events was estimated to be about 6. Therefore, in this scanning, only 3% of the located interaction events were the fake events. Since the rate of misidentification of the (K^-, K^+) event by the spectrometer was 1%, the ratio of the (K^-, K^+) vertices among all of the located ones was estimated to be 96%, which is the signal-to-backgroud ratio of our data. However, it should be noted that this ratio can be improved by repeating the emulsion scanning. Scanning is usually repeated

for important events. In this case, the probability to arrive at a fake interaction vertex becomes negligibly small. The reaction vertex position is also obtained by using the SSDs and chambers. We have compared the predicted vertex position and that actually found by an emulsion analysis. Fig.13 shows the distribution of the difference in the z-direction. Although multiple scattering in the emulsion target is very large, it is useful to compare the vertex positions for a further confirmation of the emulsion analysis.

7.3 Analysis of stopping Ξ^- events

The ionization loss of the typical Ξ^- emitted from the (K^-, K^+) interaction is about three-times larger than that of a minimum ionizing particle. It is much easier to follow Ξ^- candidate tracks in emulsion plates to their stopping or decay points than K^+ tracks. The stopping Ξ^- events are classified into ρ-stop and σ-stop categories according to its visual structure at the stopping points. The ρ-stop event has no evaporation track, except for a δ ray or blob of Auger electrons from the stopping point. The σ-stop event has some nuclear evaporation tracks from the stopping point.

We observe the stopping points with high-magnification optics in order to detect the short tracks of hyperfragments. We also apply a special process to some σ-stop events which are considered to have candidates of double hypernuclei, in order to analyze the event topology more precisely [23]. As the thickness of emulsion shrinks to about half of its original thickness after the development, the spatial resolution in an emulsion plate becomes anisotropic and degraded. In the X-Y direction (plane) it is about 0.1 μm. In the Z direction (depth) it is at least twice as bad. Moreover, due to the optical resolution of the microscope in the focusing direction, the resolution in the Z direction becomes about several μm. In order to obtain the same resolution in the Z direction, a special process is performed as follows. At first, the emulsion including the Ξ^- stopping point which we wish to analyze

is cut into the size of 3 cm × 3 cm. Then, the piece of the emulsion is swollen to about the original thickness by dipping it into water with a solution of glycerin and sugar. After swelling, the emulsion layer including the stopping point is peeled off from the polystyrene base and is sliced into a smaller size of about 500 μm × 500 μm × 1 cm. We can then measure the stopping point from four independent directions with an isotropic position resolution of 0.1 μm.

8 Summary

We have constructed an emulsion-counter hybrid detector for studying double hypernuclei and the H-dibaryon. The (K^-,K^+) reaction from the emulsion target is tagged by the K^+ spectrometer, which comprises a magnet, tracking chambers, aerogel Cherenkov detectors and a TOF hodoscope. The K^+-spectrometer has a large acceptance (0.15 str.) and detects scattered K^+ at forward angles. The K^+ is clearly identified in the mass spectrum. The ratio of misidentified particles as K^+ is less than 1%. The momentum resolution is about 2.5% at 1GeV/c, and the K^+ momentum spectrum shows a peak due to the quasifree reaction, $K^- + (p) \rightarrow K^+ + \Xi^-$.

The vertical-type emulsion stack is used as a target, and is sandwiched between SSDs having a position resolution of 16μm. The SSDs together with chambers predict the position of the K^+ track on the emulsion sheet with an accuracy of about 30μm. The efficiency to find the predicted K^+ track on the emulsion sheet was 95% at an exposed density of 9×10^5 cm^{-2} using the changeable sheet method. The error rate of the scan back of the K^+ track to the reaction vertex through the emulsion sheets was investigated. The false events due to the error were found to be only 3% among the located reaction events at this exposed density. In this detector system, the quality of the (K^-,K^+) reaction vertex found in the

emulsion can be more than 96%. We have, thus, established the method to study nuclei with S=-2 in an emulsion with both high reliability and high statistics.

9 Acknowledgements

The authors would like to acknowledge Professors H.Sugawara, K.Nakai and K.Takamatsu for their continuous encouragement throughout this work. They are greatly indebted to the staff at the KEK proton synchrotron for their support to the construction of the detector and the operation of the accelerator and the beam line. This work was supported in part by a Grant in Aid of Scientific Research on Meson Science of the Japanese Ministry of Education, Science and Culture.

References

[1] R.L.Jaffe, Phys. Rev. Lett. 38 (1977) 195.

[2] P.J.Mulders, A.T.Aerts and J.J.deSwart, Phys. Rev. D21 (1980) 2653; M.Oka, K.Shimizu and K.Yazaki, Phys. Lett. B130 (1983); A.P.Balachandran et al., Phys. Rev. Lett. 52 (1984) 887; U.Straub et al.,Phys. Lett. B200 (1988) 241; Y.Iwasaki, T.Yoshie and Y.Tsuboi, Phys. Rev. Lett. 60 (1988) 1371

[3] E.Witten, Phys. Rev. D30 (1984) 272; E.Farhi and R.L.Jaffe, Phys. Rev. D30, (1984) 2379.

[4] A Caroll et al., Phys. Rev. Lett. 41 (1978) 777; H.Ejiri et al., Phys. Lett. 228B (1989) 24; B.A.Shahbazian et al., Phys. Lett. 235B (1990) 208.

[5] M.Danysz et al., Nucl. Phys. 49 (1963) 121; D.Prowse, Phys. Rev. Lett. 17 (1966) 782.

[6] B.O.Kerbikov, Sov.J. Nucl. Phys. 39 (1984) 516.

[7] S.Aoki et al., Nucl. Instr. and Meth. A274 (1989) 64; K.Kodama et al., Nucl. Instr. and Meth. A289 (1990) 146.

[8] A.T.Aerts and C.B.Dover, Phys. Rev. Lett. 49 (1982) 1752, Phys. Rev. D28 (1983) 450.

[9] D.H.Wilkinson et al., Phys. Rev. Lett. 3 (1959) 397, A.Bechdolf et al., Phys. Lett. 26B (1968) 174.

[10] A.Yamamoto, KEK 81-13 (1981)

[11] T.Homma et al., Japanese J. of Applied Phys. 26 (1987) 602.

[12] M.Akemoto et al., Phys. Rev. Lett. 51 (1983) 1838.

[13] T.Sugitake et al., Nucl. Instr. and Meth. A249 (1986) 354.

[14] H.Wind Nucl. Instr. and Meth. 115 (1974) 431.

[15] T.Nakano PhD thesis Kyoto University (1990) (unpublished).

[16] S.Aoki et al., Phys. Rev. Lett. 65 (1990) 1729.

[17] The mechanism of (K^-, K^+) reaction has been studied by T.Iijima et al., Nucl. Phys. A546 (1992) 588.

[18] The differential cross section (lab) at forward angle of $K^- + p \to K^+ + \Xi^-$ reaction is calculated with use of existing data by C.B.Dover and A.Gal, Annals of Phys. 146 (1983) 309.

[19] J.B.England et al., Nucl. Instr. and Meth. 185 (1981); B.Hyams et al., Nucl. Instr. and Meth. 205 (1983) 99.

[20] H.Tajima et al., Nucl. Instr. and Meth. A288 (1990) 536.

[21] TKO is the KEK standard similar to FASTBUS.

[22] S.Aoki et al., Nucl. Tracks and rad. Meas. 12 (1986) 249.

[23] S Aoki et al., Prog. Theor. Phys. 85 (1991) 951, 1287.

Figure Captions

Fig.1 The 2GeV/c K^- beam line and the experimental setup. The D1,2 are dipole magnets and the Q1-7 are quadropole magnets. A beam halo is cut by a collimator, and the emulsion target and silicon micro-strip detectors are located in an alminum shield hat.

Fig.2 Overview of the K^+ spectrometer. The PC1-3 are MWPC and DC1-3 are the drift chambers. The T1,T2 and TOF hodoscope are used for time-of- flight measurements. The AC1 and AC2 are aerogel Cherenkov counters.

Fig.3 Mass spectrum of scattered particles from the emulsion target for $P_K- = 1.66 GeV/c$ in the whole momentum region (a) and in $P_K+ = 0.9 \to 1.2 GeV/c$ (b).

Fig.4 Momentum spectrum of K^+ from the emulsion target. The dotted line is obtained by a Monte-Carlo calculation for the quasi-free reaction, $K^- + (p) \to K^+ + \Xi^-$, from nuclei in the emulsion.

Fig.5 Missing-mass spectrum for the $K^- + p \to K^+ + X$ reaction. The peaks are due to Ξ^- and $\Xi^{-*}(1530 MeV/c^2)$.

Fig.6 Acceptance of the spectrometer vs the K^+-momentum.

Fig.7 Location of silicon micro-strip detectors (SSD) and the emulsion target.

Fig.8 Intrinsic position resolution of the SSD measured with the SSDs, which have much finer strips, by using beam particles.

Fig.9 Ratio of the stopping Ξ^- to the produced Ξ^- vs the thickness of the emulsion target calculated by a Monte-Calro simulation. The solid and open circles are the calculations with and without any correction due to secondary interactions of K^+ particles. The ratio saturates at an emulsion thickness of about 5cm.

Fig.10 Schematic view of the emulsion stack.

Fig.11 Schematic diagram of the data-taking system.

Fig.12 Distribution of the difference between the position of a track predicted by the SSDs and that actually observed in the emulsion for the horizontal direction (a) and the vertical direction (b). They are, practically, the position resolution of the present vertex detector system.

Fig.13 Distribution of the difference between the predicted z position of vertices (sheet number in the emulsion stack) and the observed position in the emulsion. This confirms the locationing of the (K^-, K^+) vertices in the emulsion.

Table. 1 Parameters of MWPC and DC

	active area	anode wire		anode-cathode	plane	Z-position[2]
	X x Y (cm)	dia.	spacing[1]	gap	(x,y,u)	(cm)
BPC1	8 x 6.4	10μm	1mm	4 mm	x,y	
BPC2	11.2 x 6.4	10	1	4	x,y	
BPC3	14.4 x 6.4	10	1	4	x,y	-258.7
BPC4	8.4 x 6.4	10	1	4	x,y	-36.0
PC1	14.4 x 9.6	10	1	5	x,y	+15.0
PC2	32 x 19.2	20	2	6	x,y,u	+52.7
PC3	92.8 x 51.2	20	2	6	x,y	+173.9
DC1	27 x 18	20μm	15mm	6	x,y	+21.4
DC2	154 x 115	30	11.5	6	x,y	+297.6
DC3	154 x 115	30	11.5	6	x,y	+322.1

1) The values for DC's are drift distance.
2) The distance from the center of the target to the x-plane of chambers.

Table 2. The composition of the emulsion (Fuji ET-7B)

element	weight (%)	mol (%)
Ag	45.4	11.2
Br	33.4	11.1
I	0.3	0.06
S	0.2	0.2
O	6.8	11.3
N	3.1	5.9
C	9.3	20.6
H	1.5	40.0

* At the humidity of 68%

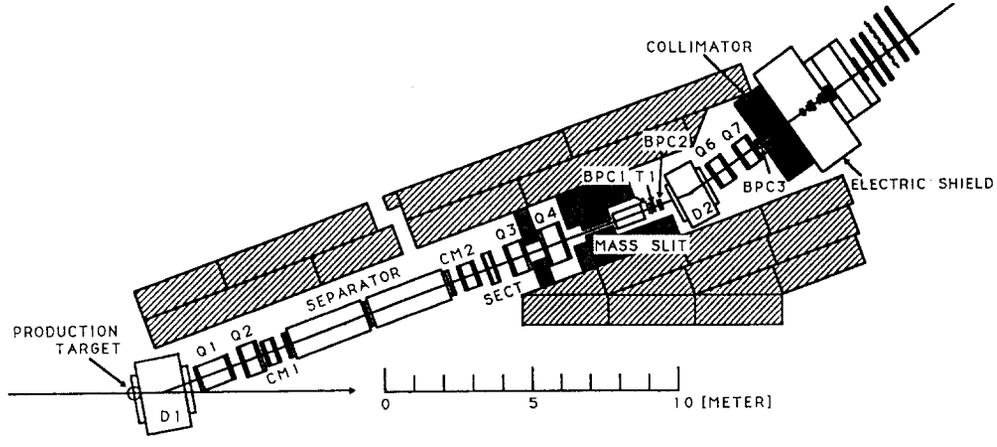

Fig. 1

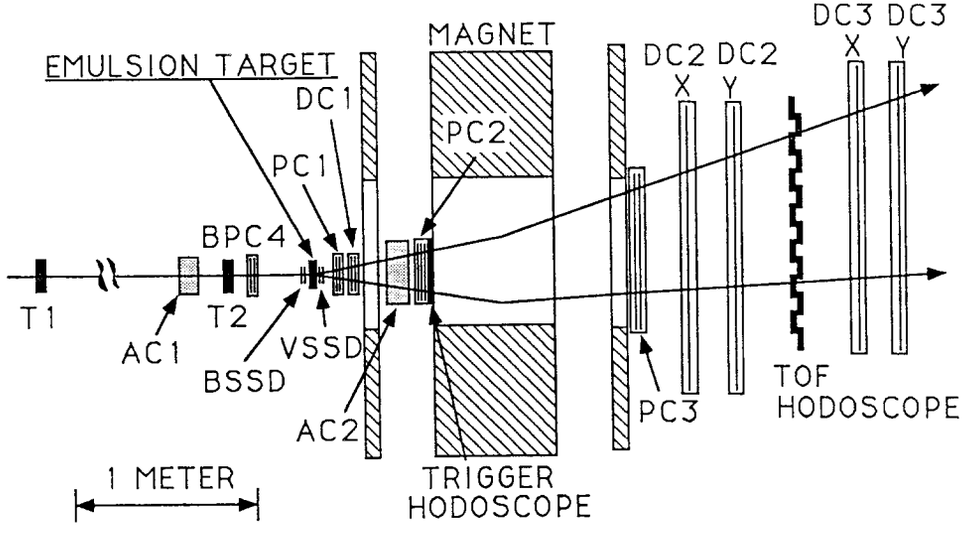
EMULSION TARGET
DC1
PC1
BPC4
T1
T2
AC1
BSSD
VSSD
AC2
MAGNET
PC2
TRIGGER
HODOSCOPE
DC2 DC2
X Y
PC3
DC3 DC3
X Y
TOF
HODOSCOPE
1 METER

Fig. 2

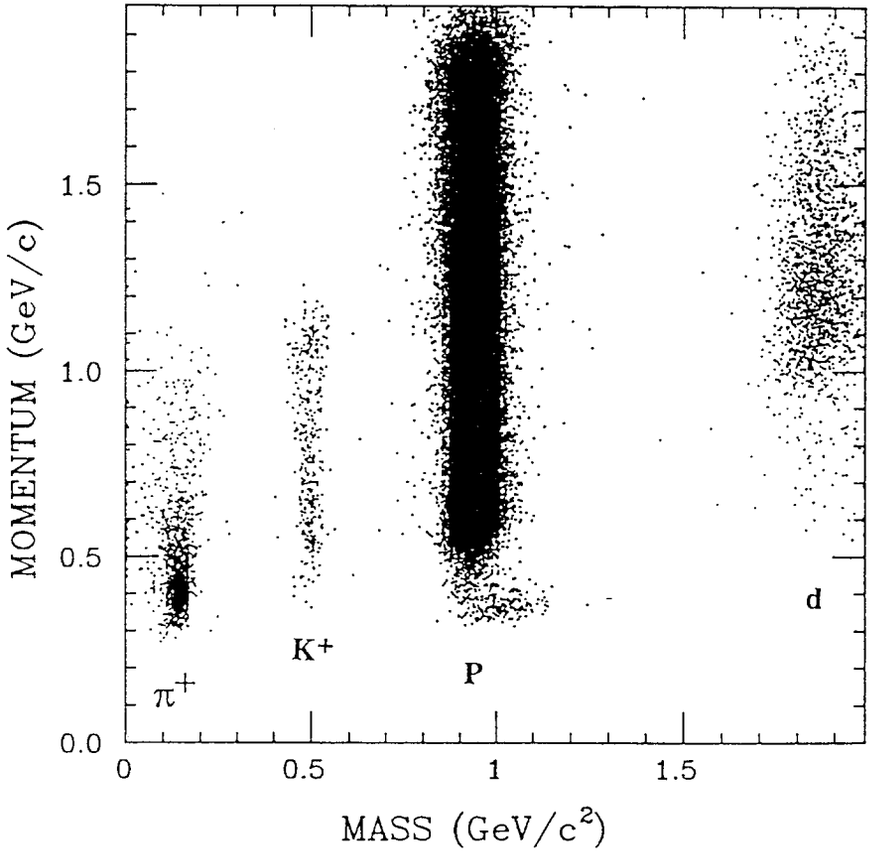
MOMENTUM (GeV/c)
MASS (GeV/c²)
0.0
0.5
1.0
1.5
0
0.5
1
1.5
π+
K+
P
d

Fig. 3(a)

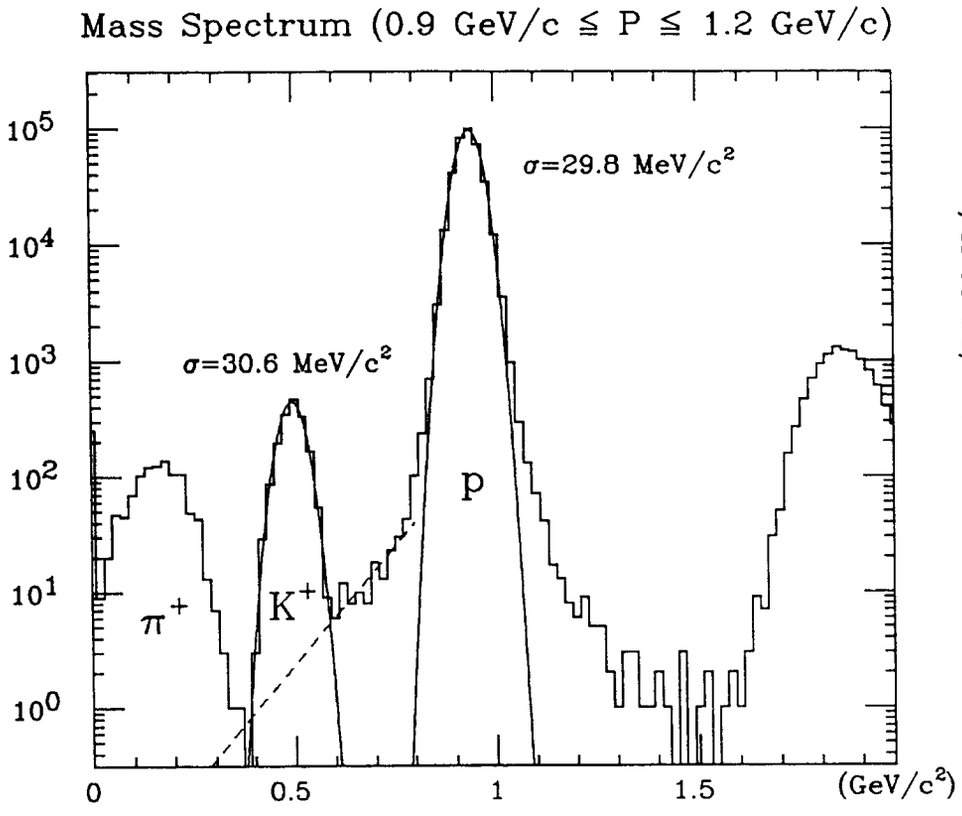
Mass Spectrum (0.9 GeV/c ≦ P ≦ 1.2 GeV/c)
σ=29.8 MeV/c²
σ=30.6 MeV/c²
p
K⁺
π⁺
10⁵
10⁴
10³
10²
10¹
10⁰
0
0.5
1
1.5
(GeV/c²)

Fig. 3(b)

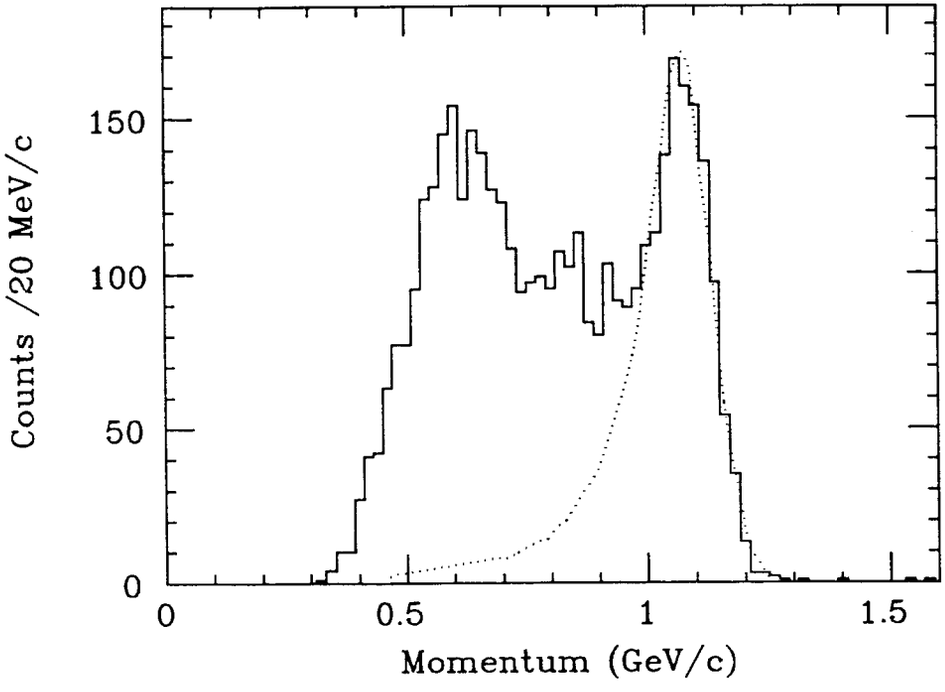
Counts /20 MeV/c
150
100
50
0
0
0.5
1
1.5
Momentum (GeV/c)

Fig. 4

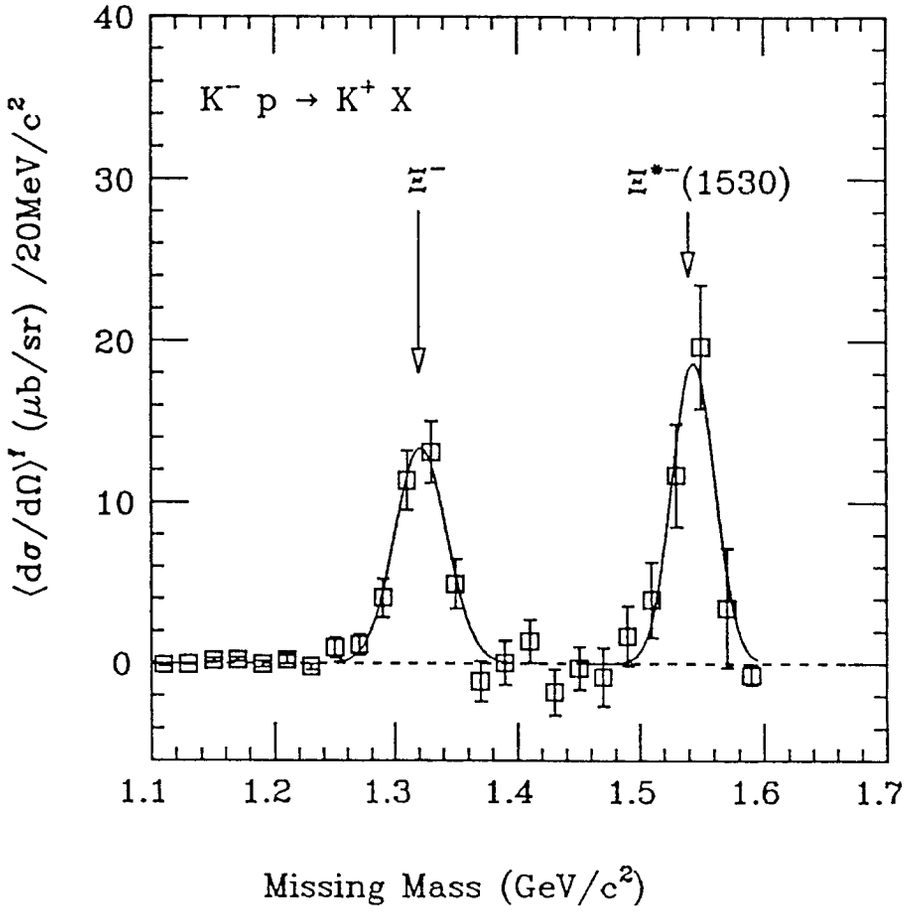
$K^- p \to K^+ X$
Ξ^-
$\Xi^{*-}(1530)$
$\langle d\sigma/d\Omega \rangle^t$ (μb/sr) /20MeV/c^2
Missing Mass (GeV/c^2)
40
30
20
10
0
1.1
1.2
1.3
1.4
1.5
1.6
1.7

Fig.5

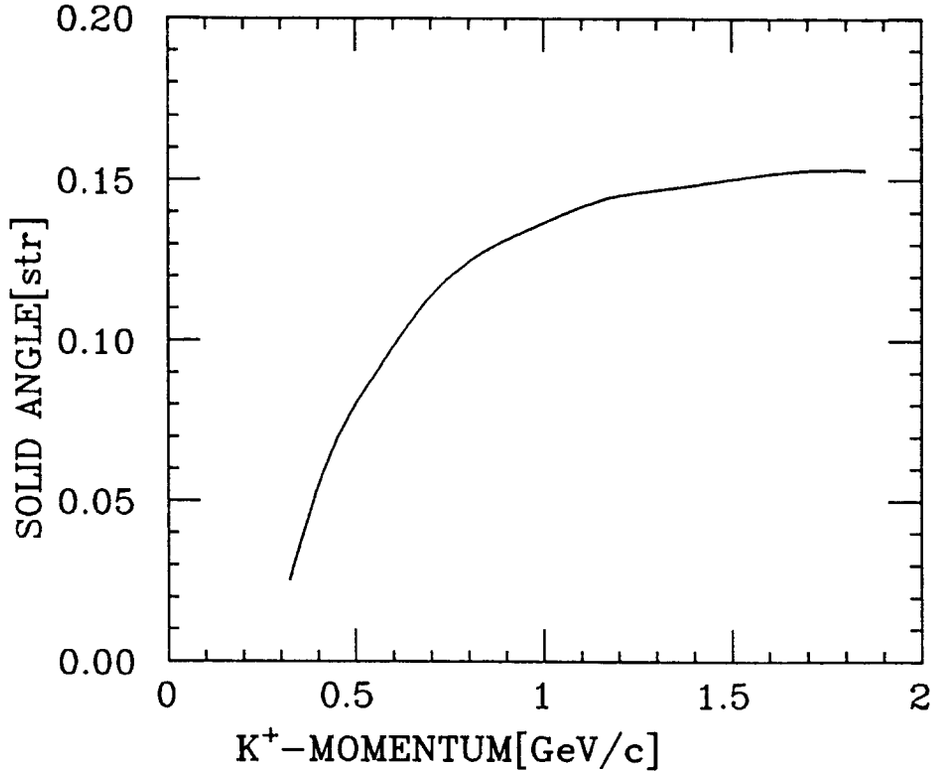
SOLID ANGLE[str]
K^+−MOMENTUM[GeV/c]
0.20
0.15
0.10
0.05
0.00
0
0.5
1
1.5
2

Fig. 6

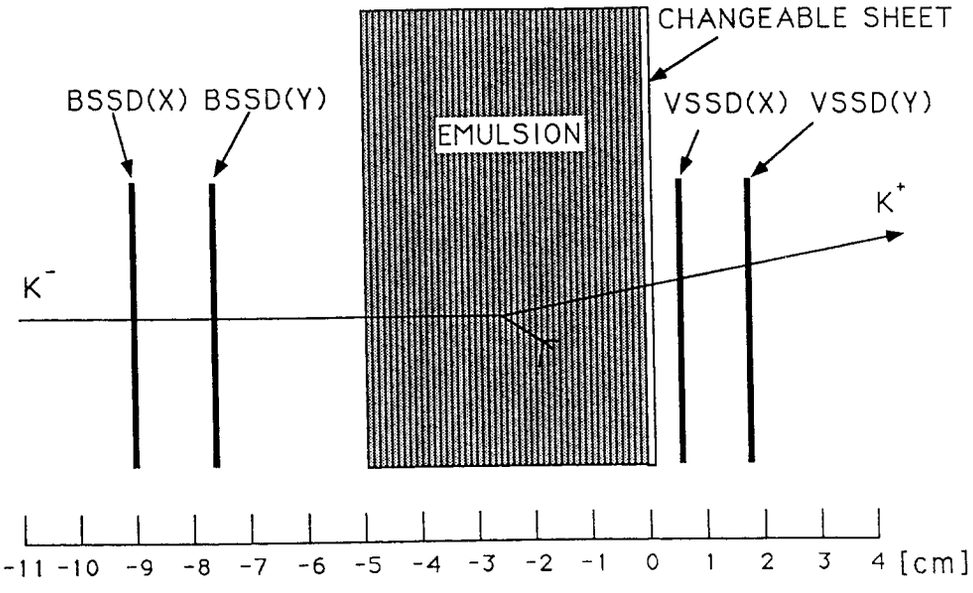
CHANGEABLE SHEET
BSSD(X) BSSD(Y)
EMULSION
VSSD(X) VSSD(Y)
K+
K-
-11 -10 -9 -8 -7 -6 -5 -4 -3 -2 -1 0 1 2 3 4 [cm]

Fig. 7

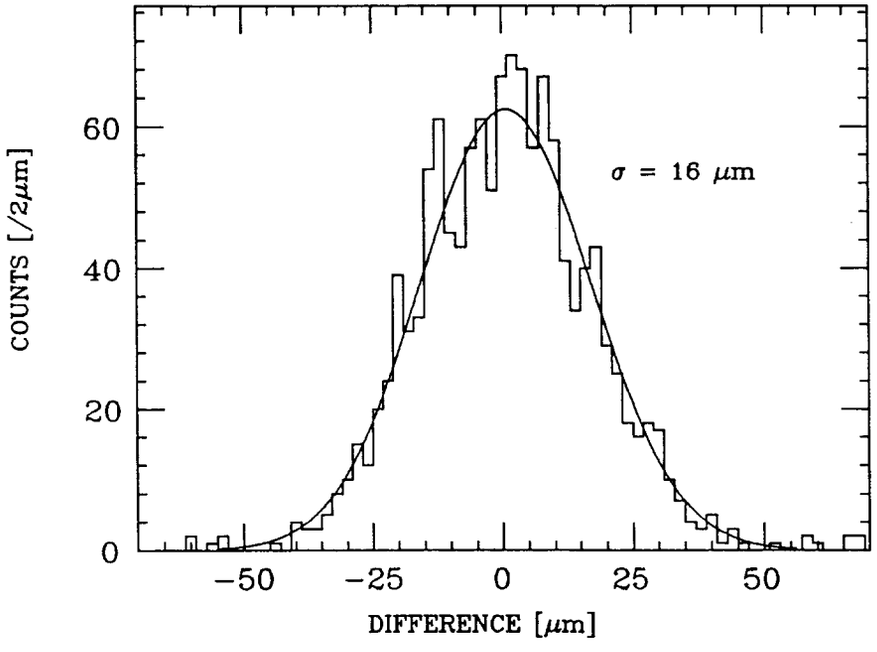
COUNTS [/2μm]
60
40
20
0
σ = 16 μm
−50
−25
0
25
50
DIFFERENCE [μm]

Fig. 8

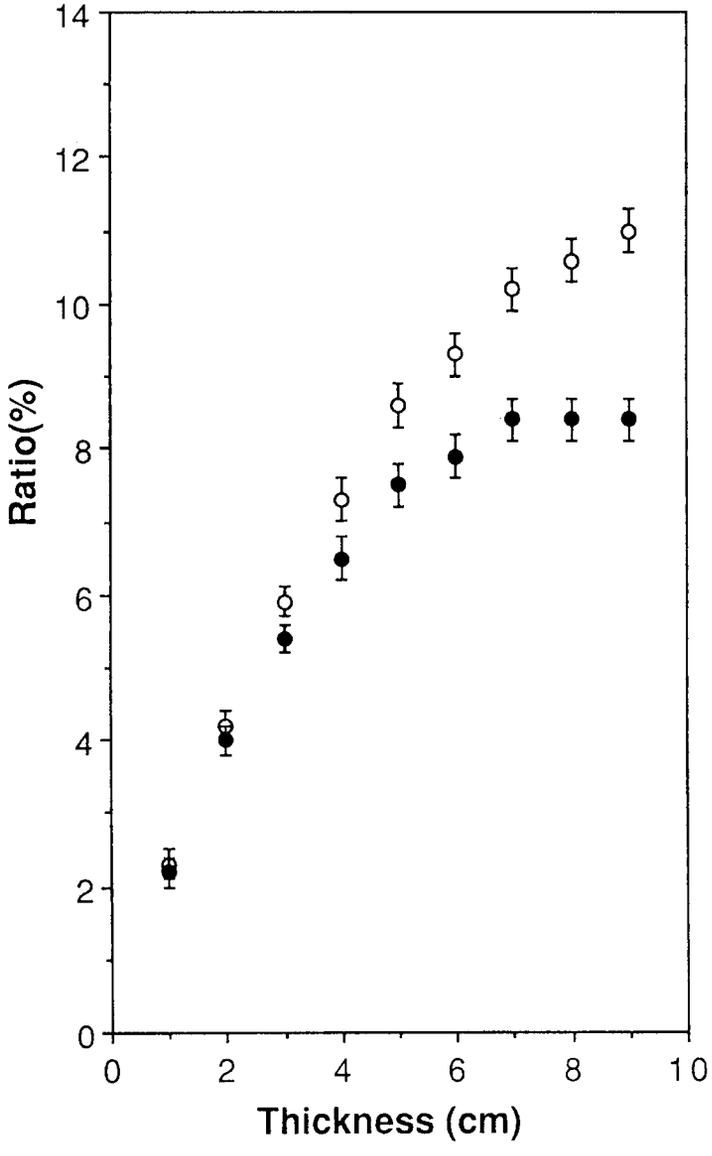
Ratio(%)
Thickness (cm)
0
2
4
6
8
10
12
14

Fig. 9

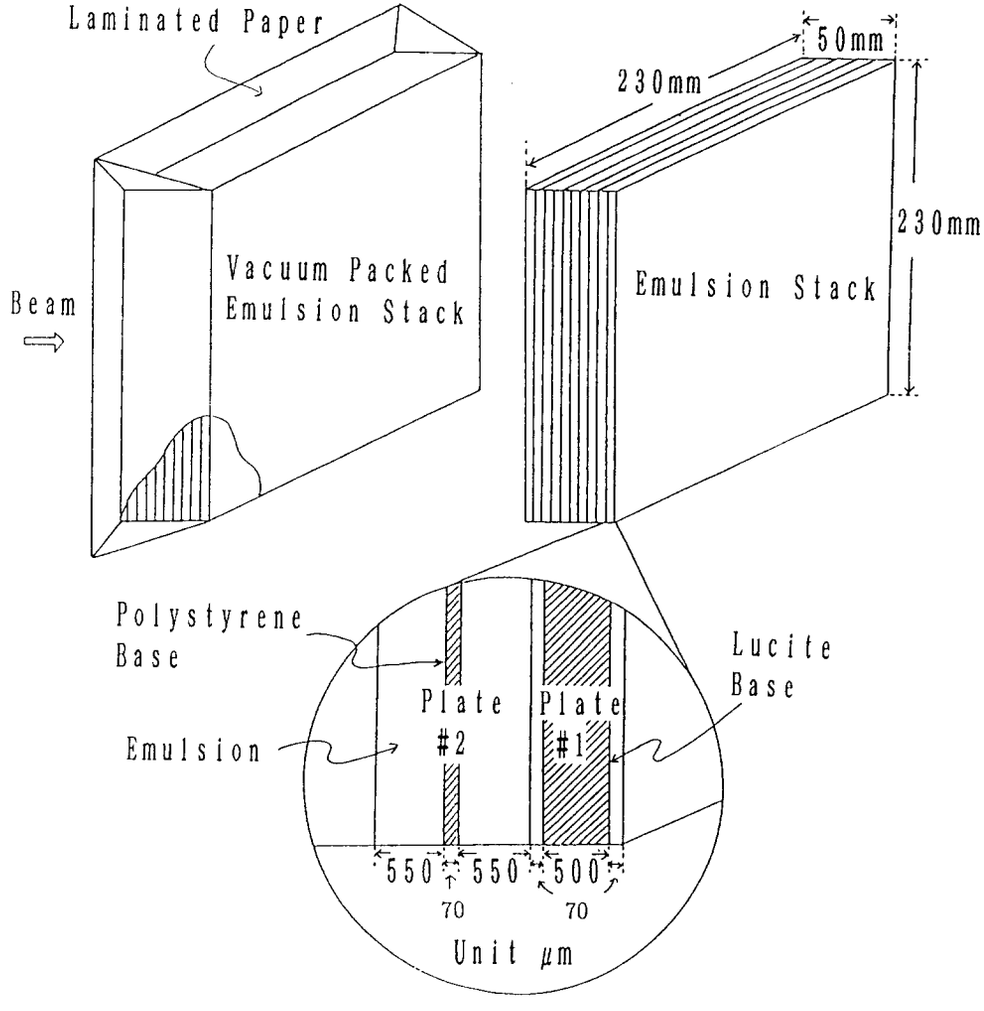
Laminated Paper
Beam
Vacuum Packed
Emulsion Stack
50mm
230mm
230mm
Emulsion Stack
Polystyrene
Base
Emulsion
Plate
#2
Plate
#1
Lucite
Base
550
550
500
70
70
Unit μm

Fig. 10

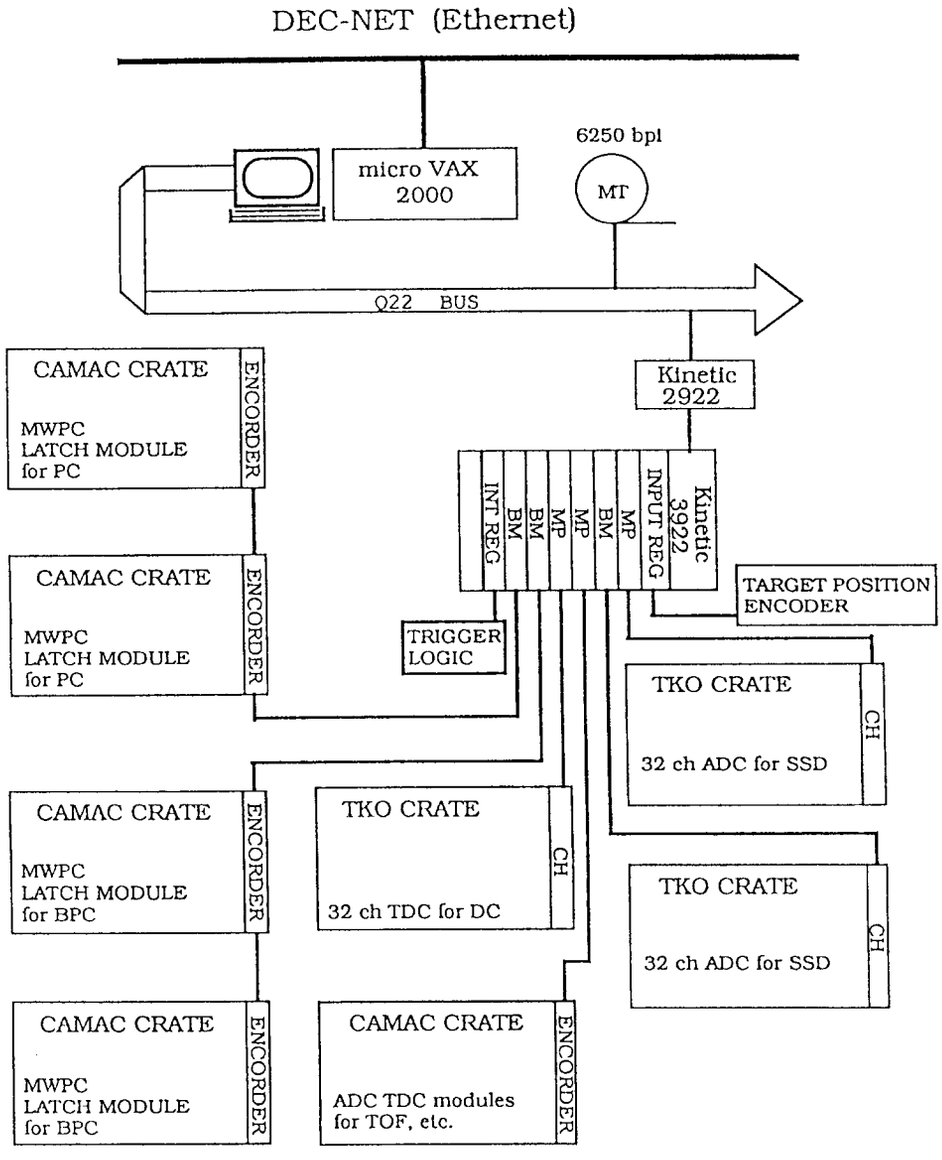

Fig. 11

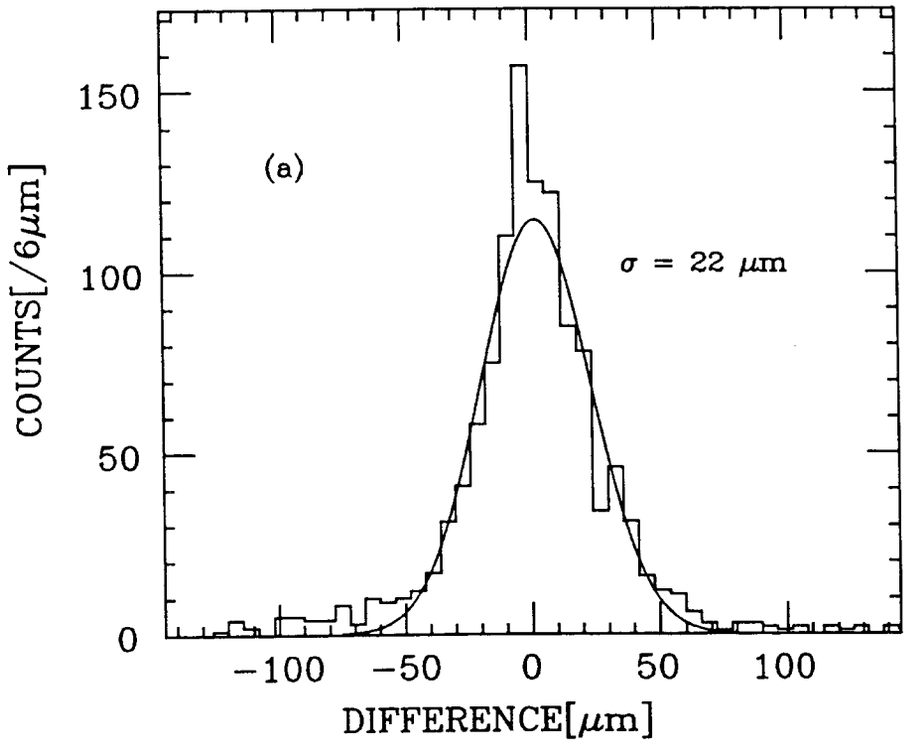

Fig. 12(a)

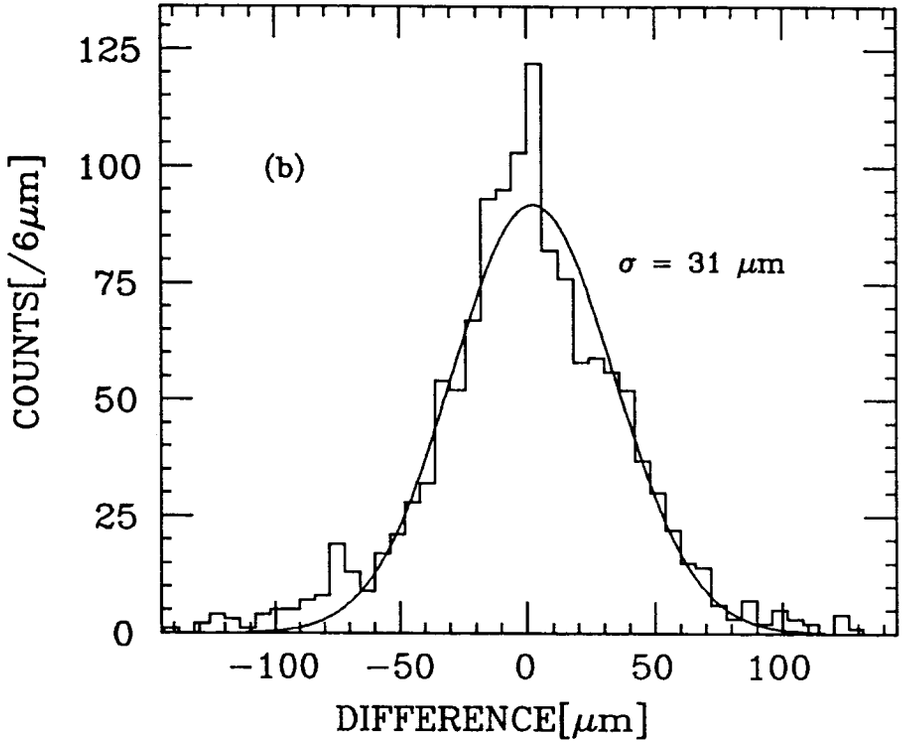

Fig. 12(b)

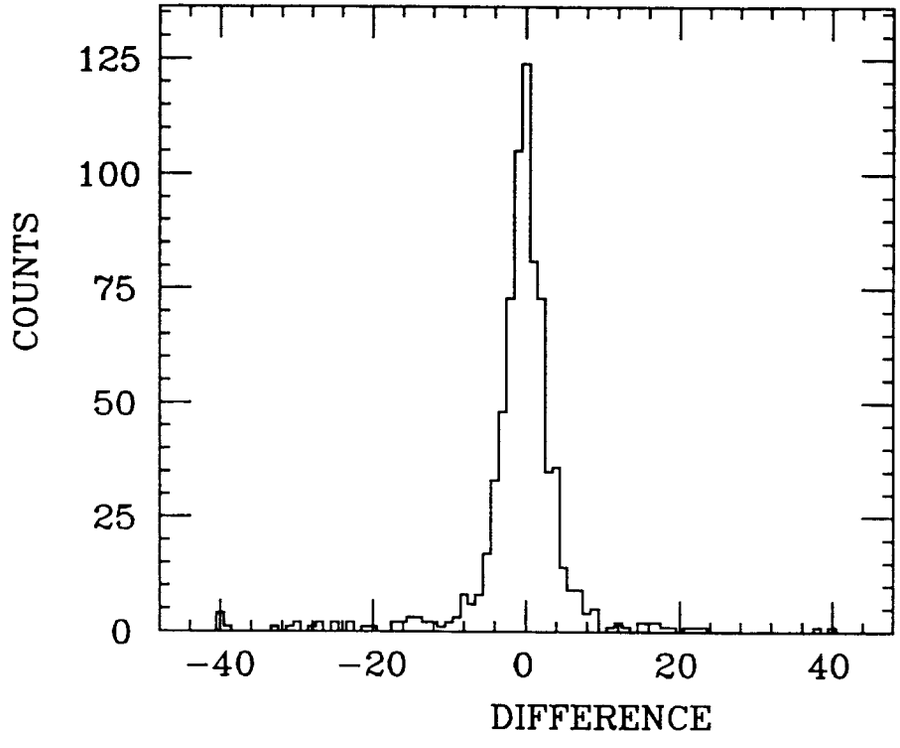

Fig. 13